Solar Energy Materials & Solar Cells 164 (2017) 13–18

Contents lists available at ScienceDirect

Solar Energy Materials & Solar Cells

journal homepage: www.elsevier.com/locate/solmat

Thickness effects of thermally evaporated C_{60} thin films on regular-type $CH_3NH_3PbI_3$ based solar cells

Kun-Mu Lee[b], Cheng-Chiang Chen[a], Lung-Chien Chen[d], Sheng Hsiung Chang[a,c,*], Kai-Shiang Chen[a], Shih-Chieh Yeh[e], Chin-Ti Chen[e], Chun-Guey Wu[a,f]

[a] Research Center for New Generation Photovoltaics, National Central University, Taoyuan 32001, Taiwan, ROC
[b] Deaprtment of Chemical and Materials Engineering, Chang Gung University, Taoyuan 33302, Taiwan, ROC
[c] Department of Optics and Photonics, National Central University, Taoyuan 32001, Taiwan, ROC
[d] Department of Electro-Optical Engineering, National Taipei University of Technology, Taipei 10608, Taiwan, ROC
[e] Institute of Chemistry, Academia Sinica, Taipei 11529, Taiwan, ROC
[f] Department of Chemistry, National Central University, Taoyuan 32001, Taiwan, ROC

ARTICLE INFO

Keywords:
C_{60} thin film
Contact angle
$CH_3NH_3PbI_3$
Solar cell

ABSTRACT

Comprehensive studies were carried out to explore the thickness-dependent characteristics of thermally evaporated C_{60} thin films. The structural, optical, electronic and surface properties of the resultant C_{60} thin films were analyzed using Raman scattering spectrometry, photoluminescence spectroscopy, absorbance spectroscopy, photoelectron emission spectrometry and water droplet contact angle measurement. The experimental results show that the thickness of the C_{60} thin film has a decisive impact on the photovoltaic performance of $CH_3NH_3PbI_3$ based solar cells in terms of open-circuit voltage (V_{OC}), short-circuit current density (J_{SC}) and fill factor (FF). In the case of the 2.5 nm-thick C_{60} film, the solar cells have the better V_{OC} and J_{SC}, as the results of the lower electron affinity and higher transparency. The FF of the solar cell is related to the coverage of C_{60} on the transparent conductive electrode (TCE) and the $CH_3NH_3PbI_3$ perovskite continuity. Consequently, the photovoltaic performance can be expected to be improved by using a smooth TCE.

1. Introduction

The existence of an icosahedral $C_{60}H_{60}$ cage was predicted in 1970 [1], which is a football-like symmetric molecule. $C_{60}H_{60}$ (C_{60}) is commonly called buckminsterfullerenes and has been widely used in optoelectronic devices [2–7] owing the superior optical and electrical properties of C_{60} thin films. A C_{60} is a non-polar molecule, which has a low solubility in organic solvents [8] and thereby impedes the formation of a high-quality C_{60} thin film. The hydrophobic nature of C_{60} molecules [9] results in the discontinuous C_{60} thin films on hydrophilic substrates when using the spin-coating deposition method. The carrier mobility in the spin-coated C_{60} thin films is low due to randomly distributed C_{60} molecules [10], which limits the device performance. C_{60} molecules have a moderate melting point (~600 °C). Therefore, a high-quality C_{60} thin film can be fabricated using the vacuum thermal evaporation deposition technique. In the reference [11], a crystalline C_{60} thin film can be obtained by means of powder sublimation (~300 °C) on quartz substrate under a ultra high vacuum (UHV) environment (10^{-7} Torr) with a slow evaporation rate at 0.01–0.02 nm/s, which results in a conduction band minimum at −4.1 eV. Before the thin-film deposition, the C_{60} (99%) powder has to be degassed at 200 °C under high vacuum environment for a several hours to remove the absorbed impurities and residual solvent. Therefore, it takes a lot of time to fabricate the high-quality C_{60} thin film by the means of powder sublimation. Thermal evaporation involves the creation of a hot source material and the deposition of a thin film on the substrate. The use of UHV in the thermal evaporation can minimize the kinetic energy loss of evaporated particles, thereby increasing the quality of deposited thin films [12,13]. The UHV thermally deposited C_{60} thin films were used in the regular-type $CH_3NH_3PbI_3$ based solar cells as the electron transporting layer (ETL), which results in a high power conversion efficiency (PCE) of 19.1% [14] due to the high electron mobility of 1.6 cm^2/Vs. The thickness of C_{60} thin films highly influences the PCE of $CH_3NH_3PbI_3$ based solar cells [15]. However, the thickness effect of C_{60} thin films on the photovoltaic performance of $CH_3NH_3PbI_3$ thin films were not comprehensively studied.

We seek to understand the thickness effects of C_{60} thin films on the photovoltaic performance of $CH_3NH_3PbI_3$ based solar cells. The correlation between the properties of the C_{60} thin films and the

* Corresponding author at: Research Center for New Generation Photovoltaics, National Central University, Taoyuan 32001, Taiwan, ROC.
E-mail addresses: shchang@ncu.edu.tw (S.H. Chang), t610002@cc.ncu.edu.tw (C.-G. Wu).

http://dx.doi.org/10.1016/j.solmat.2017.02.003
Received 10 December 2016; Received in revised form 25 January 2017; Accepted 3 February 2017
Available online 09 February 2017
0927-0248/

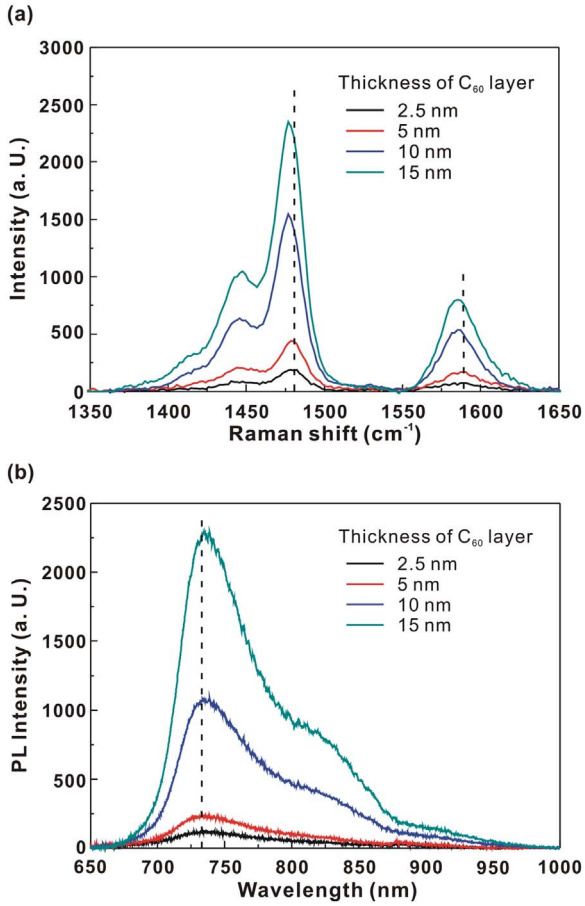

Fig. 1. (a) Raman scattering spectra of the C_{60} thin films; (b) Photoluminescence spectra of the C_{60} thin films.

photovoltaic performance of the $CH_3NH_3PbI_3$ based solar cells were investigated by the absorbance spectrometer, photoluminescence (PL) spectrometer, photoelectron emission spectrometer, Raman scattering spectrometer and contact angle measurement imaging system. In addition, the hysteresis in the current density-voltage (J-V) curves (PCE) can be reduced (improved) by using an interlayer of the compact TiO_2 thin film between the transparent conductive electrode and the C_{60} thin film.

2. Fabrication

C_{60} thin film was deposited on top of the FTO/glass substrate with a sheet resistance of 10 Ω/sq using the thermal evaporation at a rate of 0.075 nm/s under a high vacuum environment (5×10^{-6} Torr). The toluene-assisted one-step spin-coating solution process was used to fabricate the $CH_3NH_3PbI_3$ thin film on top of the C_{60}/FTO/glass. The detailed fabrication process of the $CH_3NH_3PbI_3$ thin film is described in our previous report [16]. Spiro-OMeTAD was spin coated on top of the $CH_3NH_3PbI_3/C_{60}$/FTO/glass as the hole transporting layer (HTL). Then, Ag were thermally evaporated onto the sample to act as the anode electrode. The active area (0.1 cm^2) of the solar cell was defined by using a shadow mask during Ag evaporation. The final photovoltaic structure was comprised of Ag/Sprio-OMeTAD/$CH_3NH_3PbI_3/C_{60}$/FTO/glass. The thicknesses of FTO, $CH_3NH_3PbI_3$, Spiro-OMeTAD, and Ag were controlled at ca. 400 nm, 280 nm, 150 nm, and 100 nm, respectively. The thickness of the C_{60} thin films was varied from 2.5 to 15 nm by controlling the deposition time. The J-V curves were recorded using a commercial Keithly 2400 source-measurement unit. The optical intensity of the simulated sunlight was calibrated using an NREL-certieid silicon solar cell (Oriel, 91150 V) with a KG-5 bandpass

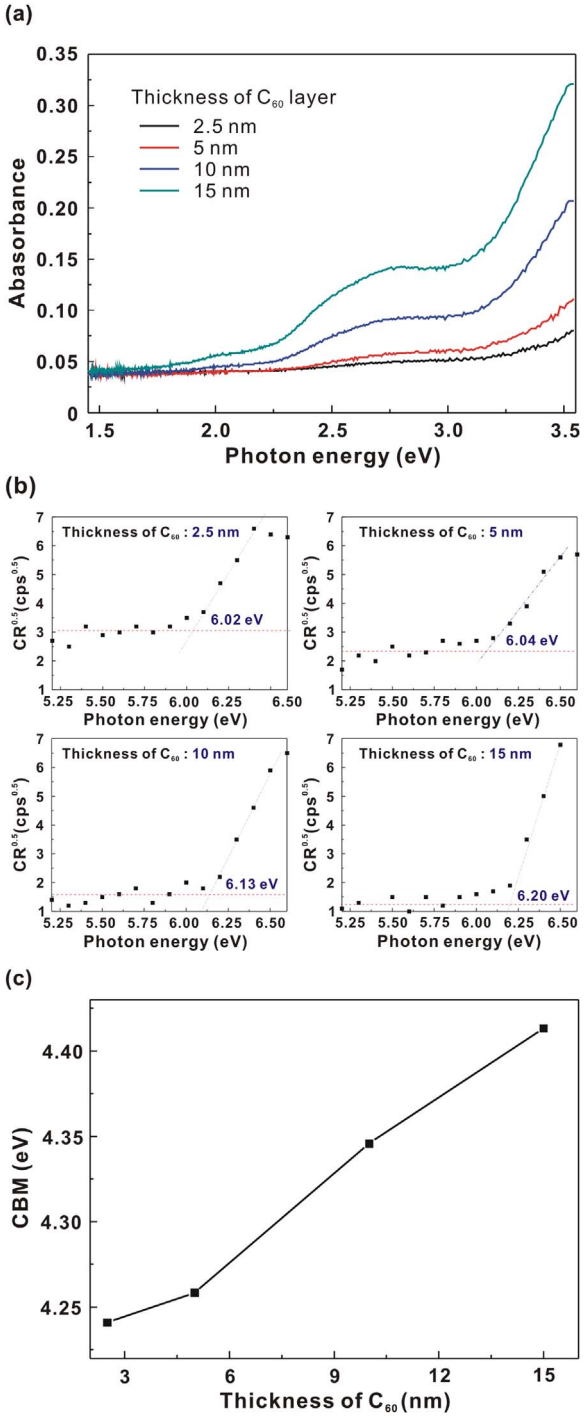

Fig. 2. (a) Absorbance spectra of the C_{60} thin films; (b) Photoelectron emission spectra of the C_{60} thin films; (c) Conduction band minimums of the C_{60} thin films.

filter to have an optical intensity of 100 mW/cm^2 (AM 1.5 G). The molecular structure of C_{60} thin films was evaluated usin the Raman scattering spectrometer and photoluminescence (PL) spectrometer (UniRAM, Protrustech). The conduction band minimum (CBM) and valence band maximum (VBM) of C_{60} thin films were determined by the combination of the absorbance spectrometer (U-4100, HITACHI) and photoelectron emssion spectrometer (AC2, Riken Keiki). The hydrophility of C_{60} thin films was assessed using a home-made contact angle image measurement system. The surface morphologies of $CH_3NH_3PbI_3$ thin films were measured by a contact-mode atomic-force microscope (E-Sweep System, Seiko).

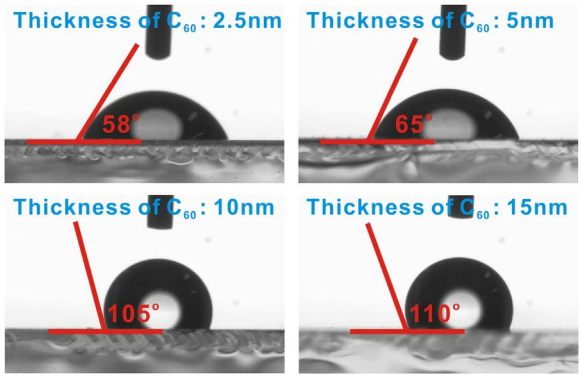

Fig. 3. Water droplet contact angle images of the C_{60} thin films.

3. Results and discussion

Fig. 1 presents the Raman scattering spectra and photoluminescence (PL) spectra of C_{60} thin films. The Raman sfhits at ~1446 cm^{-1}, ~1479 cm^{-1} and ~1584 cm^{-1} are assigned as the pinch mode (symetric Ag mode) in the disordered C_{60}, pinch mode in the ordered C_{60} and high-frequency Hg mode, respectively [11]. The pinch mode in ordered C_{60} and high-frequency Hg mode both are red-shifted, which indicates that the interaction strength between adjacent C_{60} molecules decreases with an increase in the C_{60} layer thickness. In the PL spectra, the one prominent peak (~736 nm) and two shoulders (~823 nm and ~909 nm) corresponds to the main band emission and phonon replicas of the C_{60} thin films [17]. The main band emssion peak of the C_{60} thin films is shifted from ~734 nm to ~736 nm, which indicates that the crystallinity of the C_{60} thin films increases with an increase in the C_{60} layer thickness.

Fig. 2 presents the absorbance spectra, photoelectron emission spectra and CBM energy level (E_C) of C_{60} thin films. The optical bandgap (E_g) of the C_{60} thin film can be obtained by determining the absrobance onset in Fig. 2(a), while the VBM energy level (E_V) of the C_{60} thin film can be determined by measuring the photoelectron emission spectrum as shown in Fig. 2(b). The E_C of the C_{60} thin film can be calculated by the relation: $E_C=E_V+E_g$, as shown in Fig. 2(c). The experimental results show that the E_C of the C_{60} thin film increases from −4.24 eV to −4.41 eV with an increase in the C_{60} layer thickness from 2.5 to 15 nm. The thickness-dependent electronic characteristics implies that the surface properties of the C_{60} thin films are related to the thickness. Fig. 3 presents the water droplet contact angle images of C_{60} thin films. The contact angle of the C_{60} thin film increases from 58° to 105° with an increase in the C_{60} layer thickness from 2.5 to 15 nm. There is a transition from hydrophilicity to hydophobicity when the C_{60} layer thickness increases from 5 nm to 10 nm. The thickness-depednet contact angle of the C_{60} thin film is possibly related to the interaction strength between adjacent C_{60} molecules. A thicker C_{60} thin film has a more ordered arrangement of C_{60} molecules, which results in a lower surface free energy (larger water droplet contact angle). As a result, the optical, electronic and surface properties of the thermally evaporated C_{60} thin films can be manipulated by controlling the thickness.

To further explore the influence of the thickness-dependent C_{60} thin film on the formation of $CH_3NH_3PbI_3$ thin films, the marcroscopic and microscopic images were observed as shown in Fig. 4. Fig. 4(a) presents the transparent optical (TO) images of $CH_3NH_3PbI_3/C_{60}$/FTO/glass samples, which shows that the coverage of $CH_3NH_3PbI_3$ on the C_{60}/FTO/glass in the marcroscopic scale can be optimized when the C_{60} layer thickness is 2.5 nm. When the C_{60} layer thickness is larger than 10 nm, there are a lot of sub-millimeter bright spots which corresponds the regions of the C_{60}/FTO/glass. Fig. 4(b) presents the atomic-force microscopic (AFM) images of $CH_3NH_3PbI_3/C_{60}$/FTO/glass samples. The grain size of the $CH_3NH_3PbI_3$ thin film increases from 872 nm to 2137 nm with an increase in the water droplet contact angle of the C_{60} thin film from 58° to 110°. The TO images and AFM images show that the hydrophilic (hydrophobic) C_{60} thin film is advantageous to the formation of densely packed (large grained) $CH_3NH_3PbI_3$ thin films.

In the regular-type $CH_3NH_3PbI_3$ based solar cell as shown in Fig. 5(a), the photovoltaic performance is strongly influenced by the properties of ETLs [18–20]. The sunlight has to propagate to the active layer ($CH_3NH_3PbI_3$) without significant loss in the ETL. After this, the photo-excited excitons in the $CH_3NH_3PbI_3$ thin film have to dissociate for the generation of photocurrents. The energy potential of the electrons (holes) in the ETL (HTL) determines the open-circuit voltage ($V_{OC}=E_{ETL}/e-E_{HTL}/e$) [21] as shown in Fig. 5(b), where E_{ETL} is the CBM energy level of the ETL, E_{HTL} is the VBM energy level of the HTL. It means that the regular-type $CH_3NH_3PbI_3$ based solar cell is predicted to have a higher short-circuit current density (J_{SC}) and a larger V_{OC} when a thinner C_{60} layer is used as the ETL. On the other hand, the formation of the $CH_3NH_3PbI_3$ thin film in the regular perovskite solar cell structure is highly related to the surface properties of the ETL (see Figs. 3 and 4). It means that the hydrophilic nature in the thinner C_{60} film is advantageous to the formation of a continuously $CH_3NH_3PbI_3$ thin film, which dominates the fill factor (FF) of the corresponding solar cell.

3.1. Photovoltaic performance

Fig. 6(a) presents the current density-voltage (J-V) curves of the regular-type $CH_3NH_3PbI_3$ based solar cells under the forward scan direction from −0.1 to 1.2 V. The average photovoltaic performance of 12 devices for each fabrication condition is listed in Table 1. The PCE can be dramatically improved from 0.67% to 8.54% when a 2.5 nm-thick C_{60} film was used as the ETL and hole blocking layer. The V_{OC}, J_{SC} and FF were simultaneously decreased when the C_{60} layer thickness was increased from 2.5 to 15 nm. The decrease in the V_{OC} is due to the thickness-dependent CBM of the C_{60} thin film. The trend of the reduction in the J_{SC} is inversely proportional to the absorbance of the C_{60} thin film, which indicates that the incident light absorbed by the C_{60} thin film does not contribute to the generation of photocurrents. The FF decreases from 41.2% to 29.9% with an increase in the C_{60} layer thickness from 2.5 to 15 nm, which is related to the coverage of $CH_3NH_3PbI_3$ on the C_{60}/FTO/glass sample as shown in Fig. 4(a). Fig. 6(b) presents the hysteresis behaviors in the J-V curves. The FF (PCE) of the $CH_3NH_3PbI_3$ based solar cells can be dramatically increased to 62% (12.48%) under the reverse scan direction from 1.2 V to −0.1 V, which is possibly due to the charge-detrapping result [22] at the C_{60} grain boundaries.

In order to improve the PCE of the $CH_3NH_3PbI_3$ based solar cells, a 20 nm-thick TiO_2 was deposited on top of the FTO/glass substrate as the buffer layer. Fig. 7 presents the photovoltaic performance of the $CH_3NH_3PbI_3$ based solar cells with and without the TiO_2 buffer layer. The PCE (FF) of the $CH_3NH_3PbI_3$ based solar cells can be improved from 8.54% (41.2%) to 10.02% (51.8%) when a TiO_2 thin film was used as the buffer layer, while the hysteresis in the J-V curves was reduced. The PCE (FF) was increased from 10.02% (51.8%) to 13.31% (70.6%) under the reverse scan direction from 1.2 V to −0.1 V, which indicates that the photovoltaic performance of the $CH_3NH_3PbI_3$ based solar cells can be further improved by minimizing the hysteresis in the J-V curves because the hysteresis originates from the reduction in the FF possibly caused by the charge-detrapping at the C_{60} grain boundaries.

4. Conclusions

In summary, we have studied the structural, optical, electronic and surface properties of the thermally evaporated C_{60} thin films as the n-type compact layer in the regular-type $CH_3NH_3PbI_3$ solar cell. The thickness-dependent properties of the C_{60} thin films highly influence the photovoltaic performance. The experimental results show that the

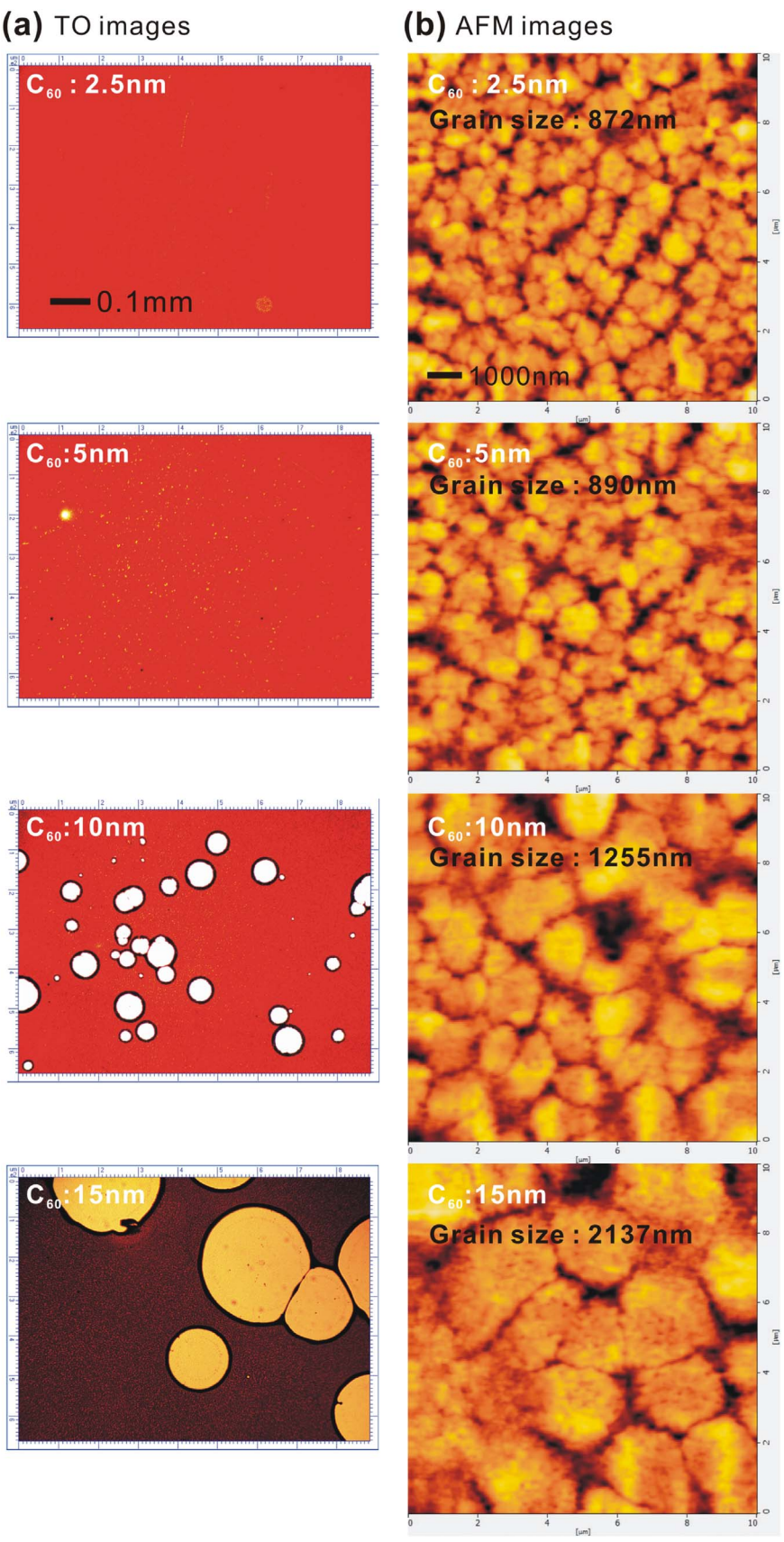

Fig. 4. (a) Transparent optical (TO) images of the $CH_3NH_3PbI_3/C_{60}$/FTO/glass samples; (b) Atomic-force microscopic (AFM) images of the $CH_3NH_3PbI_3/C_{60}$/FTO/glass samples.

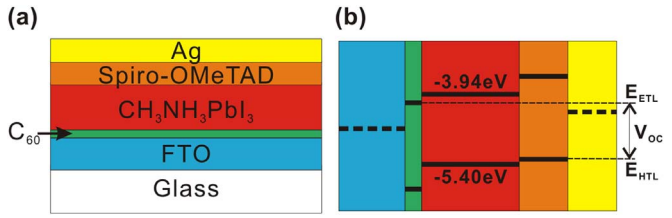

Fig. 5. (a) Schematic structure of the regular-type $CH_3NH_3PbI_3$ based solar cell; (b) Energy band diagram of the regular-type $CH_3NH_3PbI_3$ based solar cell.

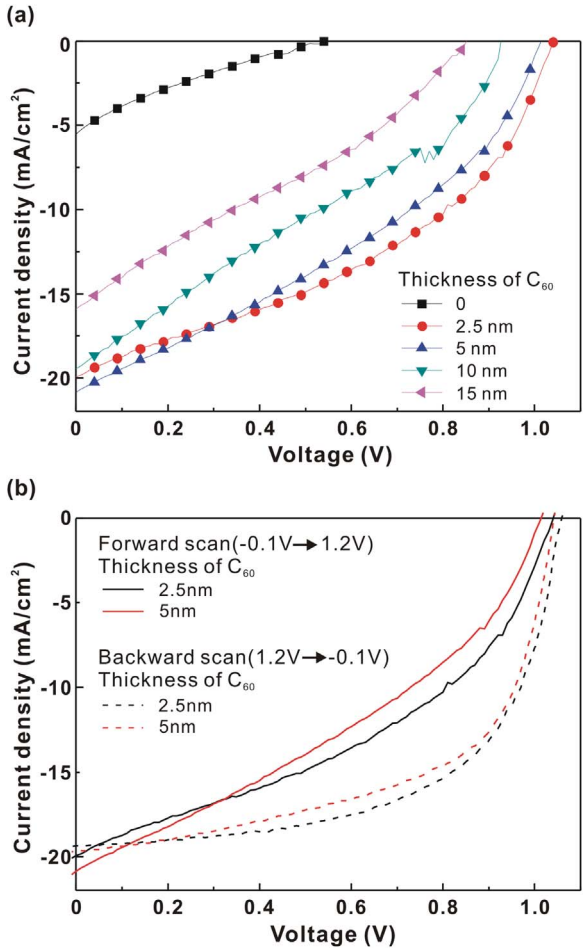

Fig. 6. (a) J-V curves of the $CH_3NH_3PbI_3$ based solar cells under the forward scan direction from −0.1 to 1.2 V; (b) Hysteresis J-V curves.

Table 1
Photovoltaic performances of the $CH_3NH_3PbI_3$ based solar cells under 1 sun illumination (AM 1.5 G, 100 mW/cm^2).

Thickness of C_{60}	V_{oc} (V)	J_{sc} (mA/cm^2)	FF (%)	PCE (%)
0 nm	0.56 ± 0.04	6.67 ± 0.82	17.9 ± 4.9	0.67 ± 0.39
2.5 nm	1.04 ± 0.03	19.93 ± 0.52	41.2 ± 0.4	8.54 ± 0.50
5 nm	1.01 ± 0.02	20.70 ± 0.21	35.3 ± 0.6	6.72 ± 0.47
10 nm	0.92 ± 0.03	19.13 ± 0.56	30.5 ± 1.3	5.37 ± 0.41
15 nm	0.85 ± 0.04	16.75 ± 1.81	29.9 ± 2.1	4.26 ± 0.40

2.5 nm-thick C_{60} film is an alternative electron selective layer in the regular-type $CH_3NH_3PbI_3$ solar cell due to the small electron affinity, high transparency and hydrophilicity surface. However, the power conversion efficiency (PCE) of the $CH_3NH_3PbI_3$ based solar cells is lower than 9% due to the small fill factor which is possibly due to the poor coverage of C_{60} on the FTO. The PCE (FF) can be increased from 8.54% (41.2%) to 10.02% (51.8%) when a 20-nm TiO_2 thin film was used as the interlayer to improve the coverage of ETL (C_{60}/TiO_2) on the FTO.

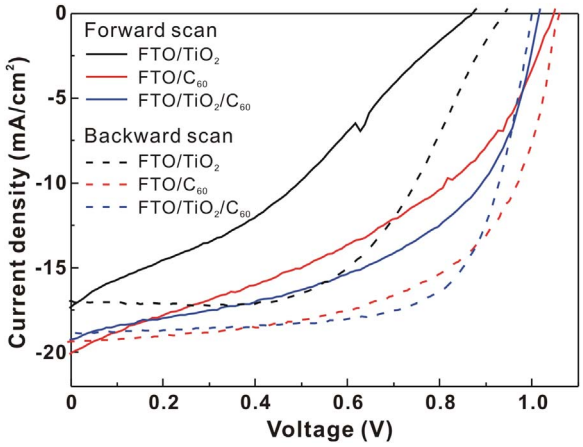

Fig. 7. J-V curves of the $CH_3NH_3PbI_3$ based solar cells with and without a 20 nm-thick TiO_2 buffer layer. The thickness of C_{60} is 2.5 nm.

Acknowledgments

This work was supported by the Ministry of Science and Technology under Grant MOST 104-2731-M-008-006-MY2. The devices fabrication was carried out in the Advanced Laboratory of Accommodation and Research for Organic Photovoltaics, Ministry of Science and Technology, Taiwan, ROC.

References

[1] E. Osawa, Superaromaticity, Kagaku 25 (1970) 854–863.
[2] N.S. Sariciftci, D. Braun, C. Zhang, V.I. Srdanov, A.J. Heeger, G. Stucky, F. Wudl, Semiconducting polymer-buckminsterfullerene heterojunctions: diodes, photodiodes, and photovoltaic cells, Appl. Phys. Lett. 62 (1993) 585.
[3] R.C. Haddon, A.S. Perel, R.C. Morris, T.T.M. Palstra, A.F. Hebard, R.M. Fleming, C_{60} thin film transistors, Appl. Phys. Lett. 67 (1995) 121.
[4] L. Ma, J. Ouyang, Y. Yang, High-speed and high-current density C_{60} diodes, Appl. Phys. Lett. 84 (2004) 4786.
[5] D. Cheyns, H. Gommans, M. Odijk, J. Poortmans, P. Heremans, Stacked organic solar cells based on pentacene and C_{60}, Sol. Energy Mater. Sol. Cells 91 (2007) 399–404.
[6] R.N. Goyal, V.K. Gupta, N. Bachheti, Fullerene-C_{60}-modified electrode as a sensitive voltametric sensor for detection of nandrolone-an anabolic steroid used in doping, Anal. Chim. Acta 597 (2007) 82–89.
[7] P. Brown, P.V. Kamat, Quantum dot solar cells. Electrophoretic deposition of CdSe-C_{60} composite films and capture of photogenerated electrons with nC_{60} cluster shell, J. Am. Chem. Soc. 130 (2008) 8890–8891.
[8] R.S. Ruoff, D.S. Tse, R. Malhotra, D.C. Lorents, Solubility of C_{60} in a variety of solvents, J. Phys. Chem. 97 (1993) (3397-3383).
[9] Y. Tajima, T. Matsuura, Y. Numata, D. Yamazaki, H. Kawamura, H. Osedo, Surface free energy and wettability determination of various fullerene derivative films on amorphous carbon wafer, Jpn. J. Appl. Phys. 47 (2008) 5730–5733.
[10] J.J. Kwiatkowski, J.M. Frost, J. Nelson, The effect of morphology on electron field-effect mobility in disordered C_{60} thin films, Nano Lett. 9 (2009) 1085–1090.
[11] K.L. Akers, C. Douketis, T.L. Haslett, M. Moskovits, Raman spectroscopy of C_{60} solid films: a tale of two spectra, J. Phys. Chem. 98 (1994) 10824–10831.
[12] Z. Zang, A. Nakamura, J. Temmyo, Single cuprous oxide films synthesized by radical oxidation at low temperature for PV application, Opt. Express 21 (2014) 11448–11456.
[13] Z. Zang, A. Nakamura, J. Temmyo, Nitrogen doping in cuprous oxide synthesized by radical oxidation at low temperature, Mater. Lett. 92 (2013) 188–191.
[14] H. Yoon, S.M. Kang, J.-K. Lee, M. Choi, Hysteresis-free low-temperature-processed planar perovskite solar cells with 19.1% efficiency, Energy Environ. Sci. 9 (2016) 2262–2266.
[15] W. Ke, D. Zhao, C.R. Grice, A.J. Cimaroli, J. Ge, H. Tao, H. Lei, G. Fang, Y. Yan, Efficient planar perovskite solar cells using room-temperature vacuum-processed C_{60} electron selective layers, J. Mater. Chem. A 3 (2015) 17971–17976.
[16] K.-F. Lin, S.H. Chang, K.-H. Wang, H.-M. Cheng, K.Y. Chiu, K.-M. Lee, S.-H. Chen, C.-G. Wu, Unraveling the high performance of tri-iodide perovskite absorber based photovoltaics with a non-polar solvent washing treatment, Sol. Energy Mater. Sol. Cells 141 (2015) 309–314.
[17] V. Gapozzi, G. Gasamassima, G.F. Lorusso, A. Minafra, R. Piccolo, T. Trovato, A. Valentini, Optical spectra and photoluminescence of C_{60} thin films, Solid State Commun. 98 (1996) 853–858.

[18] Y. Zhao, A.M. Nardes, K. Zhu, Solid-state mesostructured perovskite $CH_3NH_3PbI_3$ solar cells: charge transport, recombination, and diffusion length, J. Phys. Chem. Lett. 5 (2014) 490–494.
[19] K.-M. Lee, S.H. Chang, K.-H. Wang, C.-M. Chang, H.-M. Cheng, C.-C. Kei, Z.-L. Tseng, C.-G. Wu, Thickness effects of ZnO thin film on the performance of tri-iodide perovskite absorber based photovoltaics, Sol. Energy 120 (2015) 117–122.
[20] R. Wu, B. Yang, J. Xiong, C. Cao, Y. Huang, F. Wu, J. Sun, C. Zhou, H. Huang, J. Yang, Dependence of device performance on the thickness of compact TiO_2 layer in perovskite/TiO_2 planar heterojunction solar cells, J. Renew. Sustain. Energy 7 (2015) 043105.
[21] H.-L. Yip, A.K.-Y. Jen, Recent advances in solution-processed interfacial materials for efficient and stable polymer solar cells, Energy Environ. Sci. 5 (2012) 5994–6011.
[22] B. Chen, M. Yang, S. Priya, K. Zhu, Origin of J-V hysteresis in perovskite solar cells, J. Phys. Chem. Lett. 7 (2016) 905–917.